Kinetics of Congruent Vaporization of ZnO Islands

B. J. Kim, R. E. García, and E. A. Stach

Phys. Rev. Lett. **107**, 146101 — Published 28 September 2011

DOI: 10.1103/PhysRevLett.107.146101

Kinetics of congruent vaporization of ZnO islands

B. J. Kim[1], R. E. García[2], E. A. Stach[1†]

[1] Center for Functional Nanomaterials, Brookhaven National Laboratory, Upton, NY;

[2] School of Materials Engineering, Purdue University, West Lafayette, IN

Abstract

We examine the congruent vaporization of ZnO islands using *in situ* transmission electron microscopy. Correlating quantitative measurements with a theoretical model offers a comprehensive understanding of the equilibrium conditions of the system, including equilibrium vapor pressure and surface free energy. Interestingly, the surface energy depends on temperature, presumably due to a charged surface at our specific condition of low *P* and high *T*. We find that the vaporization temperature decreases with decreasing system size, a trend that is more pronounced at higher *T*. Applying our results of island decay towards the growth of the ZnO provides new insights into the cooperative facet growth of anisotropic nanocrystals.

† eastach@bnl.gov

Introduction

One-dimensional nanostructures of ZnO – such as nanowires, [1] nanobelts, [2] and nanotubes [3] – have attracted significant interest in the field of nanotechnology due to their potential utilization as building blocks for circuits, [4] sensors, [5] optoelectronic devices, [6] and in energy conversion [7]. To fabricate such structures, thermal growth techniques such as thermal evaporation [2] and metallorganic chemical vapor deposition [8] have been widely exploited. However, there is a significant lack of information concerning several important equilibrium physical properties of ZnO, including experimental knowledge of the equilibrium phase diagram [9], equilibrium vapor pressures [10] and surface free energies [11]. More importantly, the kinetics of both evaporation and growth has not yet been explored, largely due to the limitations of post-growth analyses.

We present quantitative measurements of congruent vaporization of nanoscale hexagonal ZnO islands formed on ZnO substrates. The islands shrink laterally, preserving their faceted shape and maintaining a constant thickness. The island area decreases smoothly with time until they reach a critical diameter (i.e., ~ 6 nm at 650 °C) at which point they shrink rapidly and vanish, indicating a strong size effect.

Using a simple kinetic model, we find that the kinetics of decomposition is consistent for all islands at a given temperature, indicating that inter-island coarsening doesn't affect the process. By fitting the model to the data, we directly obtain the equilibrium vapor pressure and surface free energy of ZnO. Intriguingly, the surface energy increases with increasing temperature, presumably because the surface is increasingly charged at low P and high T. Moreover, from the extracted parameters, we find that the vaporization temperature decreases with reductions in system size by

increasing the vapor pressure, with this trend being more pronounced at higher T. Furthermore, using the information of island decay kinetics. We find that the top and side facets grow competitively to minimize the free energy of the system, a property which displays a pressure dependence.

The ZnO vaporization experiments were carried out *in situ* to an environmental transmission electron microscope (300 kV FEI Titan ETEM, base pressure of ~ 5×10^{-7} Torr). The (0001) ZnO samples studied herein were prepared by thinning bulk wafers to electron transparency using standard methods. Details are in Suppl. Info. [19].

The ZnO islands are formed on a ZnO (0001) thin layer after annealing for about an hour at 650 °C as shown in Suppl. Fig. 1. [19] We find that ZnO decomposition initiates along the $\{10\bar{1}0\}$ prism planes, resulting in hexagonally facetted pits. These pits grow both laterally and vertically, and when impinging on each other, they create hexagonal shaped (effectively homo-epitaxial) islands. A series of representative images of the evaporation of an island (in the boxed region of Suppl. Fig. 1) with time is shown in plan view in Fig. 1(A-E). The island size decreases with time and at a visibly enhanced rate near the final moment. Fig. 1(F) schematically describes the inferred geometry of the island as a hexagonal slab with height h and, major and minor radii r_{maj} and r_{min}.

Fig. 2 (A) shows quantitative measurements of the area A versus time t of the island in Fig. 1 and several others in the neighboring areas, obtained at 650 °C. The data show that the projected area of the island decreases nearly linearly with time, until a radius $r \leq 3.1$ nm is reached. At this transition point, the island shrinks rapidly and disappears. This behavior can be related to the increasing chemical potential of the ZnO island as it shrinks (analogous to the Gibbs-Thomson effect), which destabilizes a very

small particle [12]. From contrast measurements [19] we realize that the height of the island is nearly constant during decomposition, indicating that the $\{0001\}$ top facet is nearly flat and not strongly affected by the Gibbs-Thomson effect. Thus it can be considered (to first order) that the island decay occurs solely from the $\{10\bar{1}0\}$ side facets.

To quantify and test this interpretation, we derive a simple model that describes the evolution of the linear dimension *r*, radius of the side facets of the island as a function of time. For this, we directly substitute the well-known Gibbs-Thomson relation for the vapor pressure of Zn and O into the Hertz-Knudsen equation. [12, 13] Assuming that the kinetics of island decay does not involve island interactions (i.e., coarsening), we find

$$\frac{dr}{dt} = \Omega K_n P_o \left[1 - Exp(\frac{\gamma_r \Omega}{RTr}) \right] \qquad \text{(Eq. 1)}$$

which can be reorganized to have the form for *A* vs. *t*: $\frac{dA}{dt} = 2(A/\pi)^{1/2} \Omega K_n P_\circ [1 - Exp(\frac{\gamma_r \Omega}{RT(A/\pi)^{1/2}})]$, with $r = (A/\pi)^{0.5}$. Here, Ω is the molar volume of ZnO, $K_n = \left(\frac{m}{2\pi RT} \right)^{0.5}$, *m* is the molar mass of ZnO, *R* is the gas constant, *T* is annealing temperature, P_o is total, zero curvature, equilibrium vapor pressure of Zn and O, and γ_r is the surface energy of $\{10\bar{1}0\}$ ZnO facets. The two parameters controlling the kinetics of island decay in Eq. (1) are thus P_o and γ_r, allowing us to directly determine these two important physical parameters for ZnO at our specific conditions. P_o is fitted to the linear regime of the decay, and γ_r is fitted to the final decay transition, thus determining the sharpness of the transition point. Note that Ω and K_n are known material constants.

Although the model is highly simplified, Eq. (1) gives an excellent description of the data, as illustrated in Figure 2 (A). We measured the decay of sixteen islands, with radii ranging from 6.8 nm to 17.8 nm, over temperatures from 625 °C to 700 °C. The complete set of data, and fits to Eq. (1), are shown in Suppl. Fig. 3. [19] After fitting each curve independently, we confirm that the resulting values for P_o and γ_r are consistent for all islands at a given temperature. This confirms that the island decay dominates over island interactions, and that the evaporation progresses at a virtually identical effective temperature. We estimate the uncertainty in the determined values of P_o and γ_r to be ± 5 – 10 %.

We now discuss the numerical values and physical significance of these fitted parameters as a function of T. First, we can find the enthalpy of vaporization, ΔH using the Clausius-Clapeyron relation [13], with our fitted values of P_o. Fig. 2(B) shows the relative equilibrium vapor pressure, P/P_o plotted as a function of $1/T$. From the slope of the least-squares fit, we have $\Delta H/R$, and thus a ΔH of 240 KJ/mol.

The temperature dependence of surface energy, γ_r shown in Fig. 2(C) is intriguing. It can be seen that the surface energy increases by roughly a factor of two with an increase in T of ~ 100 °C. Moreover, we recognize that the values of surface energy are much higher (over 4 ~ 7 times), compared to ones measured at room temperature. [11] This dependence is contrary to the general characteristic of most materials, where the surface energy negatively depends on temperature, due to the increasingly strong effect of entropy at elevated temperature. [14] We speculate that the temperature-dependent surface energy is attributed to our experimental condition – a low pressure and a high temperature: this could intensify the effect of surface charging,

[15] because the amount of ZnO evaporated into Zn^+ and O^- is larger than for high *P* and low *T*. Specifically, this charging effect could appear when unequal number of the two species are present on the surface. We postulate that Zn^+ left behind during evaporation is incorporated into the surface of ZnO bulk, as indicated in prior reports. [16]

It is also interesting to quantify the size dependence of the total vapor pressure of Zn and O, and to examine how this affects its vaporization temperature as a function of *T*. Fig. 3(A) presents the plots of *r* vs. P_V as a function of temperature, with the fitted values of P_o and γ_r, and using Gibbs-Thomson relation,

$$P_V = P_o \, Exp\left(\frac{\Omega\gamma_r}{RTr}\right) \qquad \text{(Eq. 2)}$$

It can be seen that the vapor pressure, P_V increases with decreasing island size due to the Gibbs-Thomson effect, and the size dependence dramatically increases with increasing *T,* owing to the increased surface energy.

Similar to Fig. 3(A), the size dependence of the vaporization temperature relative to the bulk (T_r/T_{bulk}) is plotted in Fig. 3(B). For the plots presented, we use a simple relation with the acquired values of γ_r and ΔH, [19]:

$$\frac{T_r}{T_{r=\infty}} = 1 - \frac{\gamma_r \, \Omega}{\Delta H \, r} \qquad \text{(Eq. 3)}$$

These plots demonstrate that the vaporization temperature T_r decreases with decreasing island size, caused by the pressure effect mentioned above, and this trend is even more pronounced at higher *T* with increased surface energy, as expected. As a way to consider this data, it can be seen that reductions in island sizes to 1.2 – 2.1 nm at temperatures of 625 – 700 °C causes a reduction of the congruent vaporization *T* by ~ 20% from the bulk value.

As a Gedanken experiment, if we were to reverse course and provide Zn and O in the vapor phase to a ZnO (0001) substrate, then hexagonal ZnO islands would nucleate and grow in the Volmer-Weber mode. [18] Upon first glance, one might expect the island to grow in exactly the opposite fashion as our observations of evaporation, having only lateral growth at constant height. However, such a simple mechanism is only operative during island decay, because the top face is flat and the side face has a negative curvature: this curvature increases the free energy of the island due to the Gibbs-Thomson effect, allowing the island to decay exclusively laterally with no energy barrier. However, in the case of growth, the increased free energy of the side face would prohibit the island from growing laterally. Instead, it would create a free energy barrier for nucleation. In the mean time, the top facet would grow more easily than the side facets if the total pressure of Zn and O is higher than the equilibrium vapor pressure at the given growth temperature.

To examine the above situation, we present a simple relation to explain the growth kinetics of the hypothetical island by comparing the growth rates of the top and side facets. We find:

$$\frac{dh}{dr} = \frac{P_{Zn+O} - P_o}{P_{Zn+O} - P_o Exp\left(\frac{\Omega \gamma_r}{RTr}\right)} \qquad \text{(Eq. 4)}$$

where P_{Zn+O} is the total pressure of Zn and O introduced into the growth chamber. Using the values for P_o and γ_r we determined above, we compute the relative growth rate of radius r and height h at 650 °C, shown in Fig. 4(B) by varying P_{Zn+O} from 10^{-2} to 10^{3} Torr. The growth of the island initiates at a radius r^* (the critical nucleus size) larger than zero, and at this size the top facet thickens abruptly. Subsequently, the ratio of growth rates of the two facets slows down and remains nearly constant. It is clear from

the plots that the initial size r and the jump height h decrease with increasing source pressure.

We interpret this behavior by calculating the free energy of the island. The dependence of free energy F on radius r is illustrated in Fig. 4(A) at the corresponding pressures to Fig. 4(B). Considering the geometry of the island as a hexagonal slab with the h relative to r in Fig. 4(B), we can write an equation for F vs. r which gives:

$$F = \pi r\left(ghr + 2h\gamma_r + r\gamma_h\right) \qquad \text{(Eq. 5)}$$

where g is the standard bulk Gibbs Free energy of transformation for ZnO crystal and γ_h is the surface energy of the top facet, ZnO (0001) in this case. [20]

From these results, we can categorize the free energy into three regimes based on source pressure. In the low pressure regime (below 1 Torr), an island embryo needs to overcome a kinetic energy barrier for nucleation, after which the island sees an abrupt decrease in free energy. This behavior indicates that the nucleation barrier at the critical size, r^* is imposed by the Gibbs-Thomson pressure, following which the energy barrier suddenly decreases by vertical growth of the island. After this sudden decrease, the free energy decreases slowly due to competing growth of the top and side facets, as discussed above. Importantly, the initial nucleation barrier F_I and the critical nucleus size r^* decrease with increasing gas pressure. This leads to a reduced contribution for vertical growth, as shown in Fig. 4(B). The blue plot presents the dependence of the initial nucleation barrier F_I on pressure.

At intermediate pressures (1 ~ 3 Torr), a subsequent nucleation barrier F_S appears along with the initial one, F_I. The creation of the second barrier can be explained by an increasing contribution of lateral growth relative to vertical growth at increased pressure. Within this regime, the former barrier is still larger than the latter. The second

nucleation barrier (F_S) becomes larger with increasing pressure, while the first one (F_I) becomes smaller. However, at high pressures (above 3 Torr), the second barrier overwhelms the first one, and thus controls the nucleation of the island. Importantly – in contrast to the behavior in the low temperature regime – the nucleation barrier and the critical nucleus size increase with increasing pressure (inset of Fig. 4(A)). [19]

In conclusion, quantitative *in situ* measurements combined with theoretical modeling allows us to obtain essential physical parameters for nano-size ZnO islands at equilibrium, including the equilibrium vapor pressure and surface free energy. Unexpectedly, we find that the surface energy increases with temperature, possibly due to the presence of significant surface potential at our specific condition of low P and high T. From the results, we realize that congruent vaporization temperature decreases by reducing system size due to increasing vapor pressure, and it is exaggerated at higher T. Relating our results of decay to growth of ZnO islands allows insights into unique features concerning the thermodynamics and kinetics of anisotropic crystal growth in nanoscale systems.

Acknowledgement

This work was partially funded by NSF under Grants No. DMR 0606395 and DMR 0907483. Research was also carried out in part at the Center for Functional Nanomaterials, Brookhaven National Laboratory, which is supported by the U.S. Department of Energy, Office of Basic Energy Sciences, under contract DE-AC02-98CH10886.

Figure captions

Fig. 1

(A-E) Images of the decaying island (in the boxed region in **Suppl. Fig. 1**) acquired at time specified in seconds. The scale bar is 15 nm. **(F)** Idealized schematic of the inferred geometry.

Fig. 2

(A) Linear dimension A (πr^2) of the projected area with time t for islands of different initial radii at 650 °C. The island image is approximated by an ellipse to reasonably account for the size effect of the side facets; r is calculated as the geometric mean of the semi-major and semi-minor axes, i.e. the radius of a circle with equivalent area. (See Fig. 1 (F)) Curved lines are Eq. (1) with essentially the same values of fitting parameters: P_o =1.11×10^{-6} Torr and γ_r =5.71 J/m^2. Inset (upper right) shows an expanded view of final stage of the largest island (black data plot), with a dotted vertical line to indicate the stability limit. **(B)** Relative equilibrium vapor pressure, $P_o/P_{o(625°C)}$ plotted as a function of *1/T*. **(C)** Plot of γ_r vs. T. These values in (**B** and **C**) are determined by fitting the entire data sets shown in **Suppl. Fig. S2 (A-D)**.

Fig. 3

(A) Plots of r vs. P_V (total vapor pressure) at varied T (625 – 700 °C from black to purple) with the fitted values of P_o and γ_r, and using the Gibbs-Thomson relation in Eq. (2). **(B)** Plots of r vs. T_r/T_{bulk} at the corresponding temperatures to **(A)** (plots depicted with same colors) illustrating possible changes in the phase diagram.

Fig. 4

(A) Free energy F vs. r at 650 °C with varying P_{Zn+O} during the growth of a ZnO island. Curves from right to left are, respectively, for P_{Zn+O}: 10^{-2}, $10^{-1.5}$, 10^{-1}, $10^{-0.5}$, 10^{0} (purple), $10^{0.5}$ (pink), 10^{1} and 10^{3} Torr. Low pressure regime (below 1 Torr) is for the plots to the right from the purple one, high pressure regime (above $10^{0.5}$ Torr) is for the plots to the left from the pink one, and the intermediate regime is in between purple and pink plots. The blue plot presents F_I vs. pressure. The inset is a magnified view of the intermediate and high pressure regimes where the second nucleation barrier appears. **(B)** Plots of radius r and height h at 650 °C with pressures corresponding to **(A)**. Parameters are for 650 °C as in Fig. 2(a), see text for details.

References:

[1] M. H. Huang et. al., Science **292**, 1897 (2001).

[2] Z. W. Pan et. al., Science **291**, 1947 (2001).

[3] J. J. Wu, S. C. Liu, C. T. Wu, K. H. Chen, L. C. Chen, Appl.Phys. Lett. **81**, 1312 (2002).

[4] Y. Cui and C. M. Lieber, Science **291**, 851 (2001).

[5] M. S. Arnold, P. Avouris, Z. W. Pan, Z. L. Wang, J. Phys. Chem. B **107**, 659 (2003).

[6] X. F. Duan, Y. Huang, R. Agarwal, and C. M. Lieber, Nature, **421**, 241 (2003).

[7] Z. L. Wang, J. H. Song, Science, 312, 242 (2006)

[8] W. Lee, M. C. Jeong and J. M. Myoung, Nanotechnology, **15**, 254 (2004).

[9] H. A. Wriedt, Alloy Phase Diagrams **8**, 167 (1987).

[10] D. F. Anthrop, A.W. Searcy, J. Phys. Chem. **68**, 2235 (1964); R. Helbig, J. Cryst. Growth **15**, 25 (1972).

[11] A. Wander et. al. Phys. Rev. Lett., **86**, 3811 (2001).

[12] J. W. Christian, *The Theory of Transformations in Metals and Alloys* (Pergamon, Oxford, 2002).

[13] R. T. Dehoff, *Thermodynamics in materials science* (CRC Press, 2006)

[14] T. Tokoro et. al., *Annual Report Conference*, IEEE, **316** (2007); F. Spaepen, Sol. Stat. Phys. **47**, 181 (1994).

[15] Y. I. Tarasevich, Theo. & Exp. Chem. **42**, 145 (2006); I. V. Obreimov et. al., Inv. in Exp. Theo. Phys., in Russian, 159 (1959).

[16] P. Erhart et al., Appl. Phys. Lett. **88**, 201918 (2006).

[17] A. Paul et. al., J. of Mat. Sci. **27**, 1716 (1992); E.A.Secco, Can. J. Chem. **38**, 596 (1960)

[18] J. B. Baxter, F. Wu, E. S. Aydil, Appl. Phys. Lett. **83**, 3797 (2003).

[19] Supplementary materials.

[20] From the literature, we obtain g =114640-51.65T (cal/mol) [17] and $\gamma_h \sim 1.724\,\gamma_r$ at equilibrium [11].

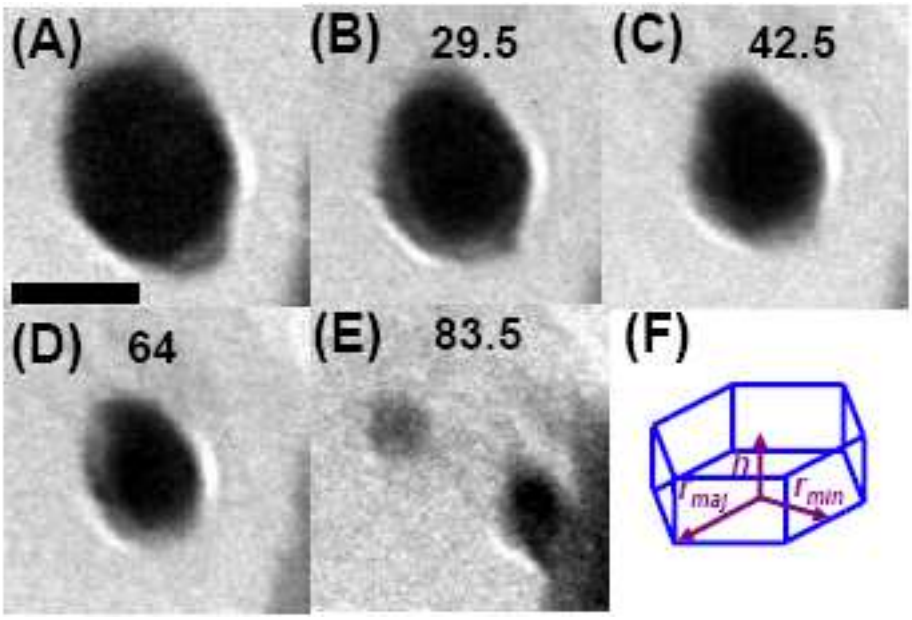

Figure 1 LE13579 04AUG2011

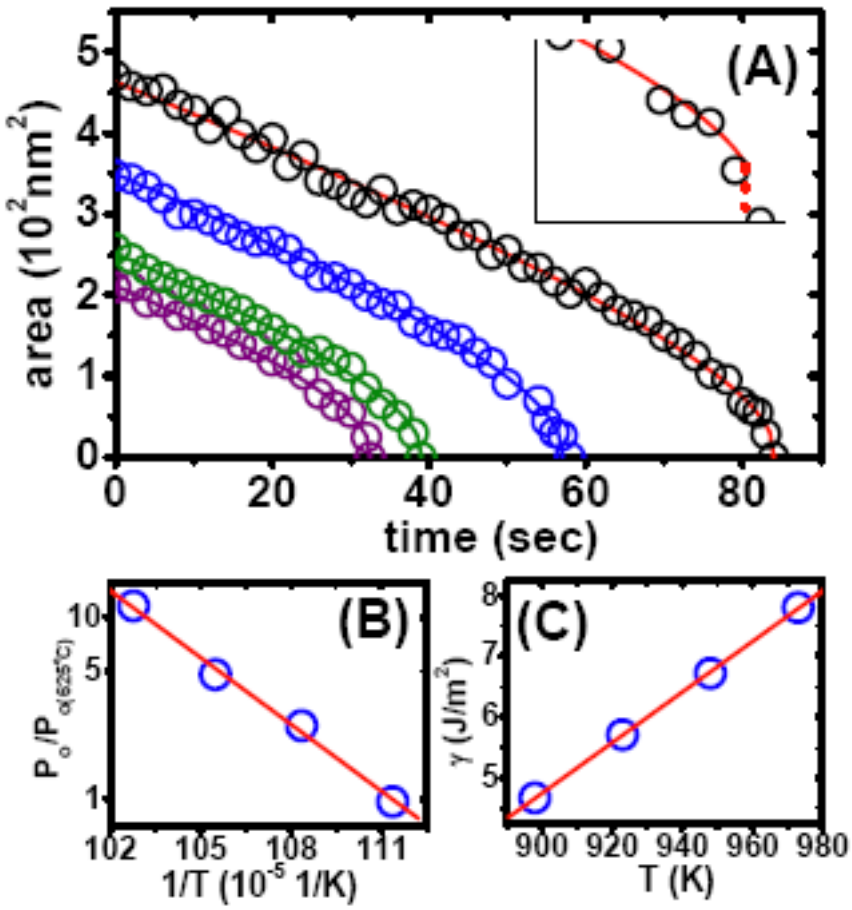

Figure 2 LE13579 04AUG2011

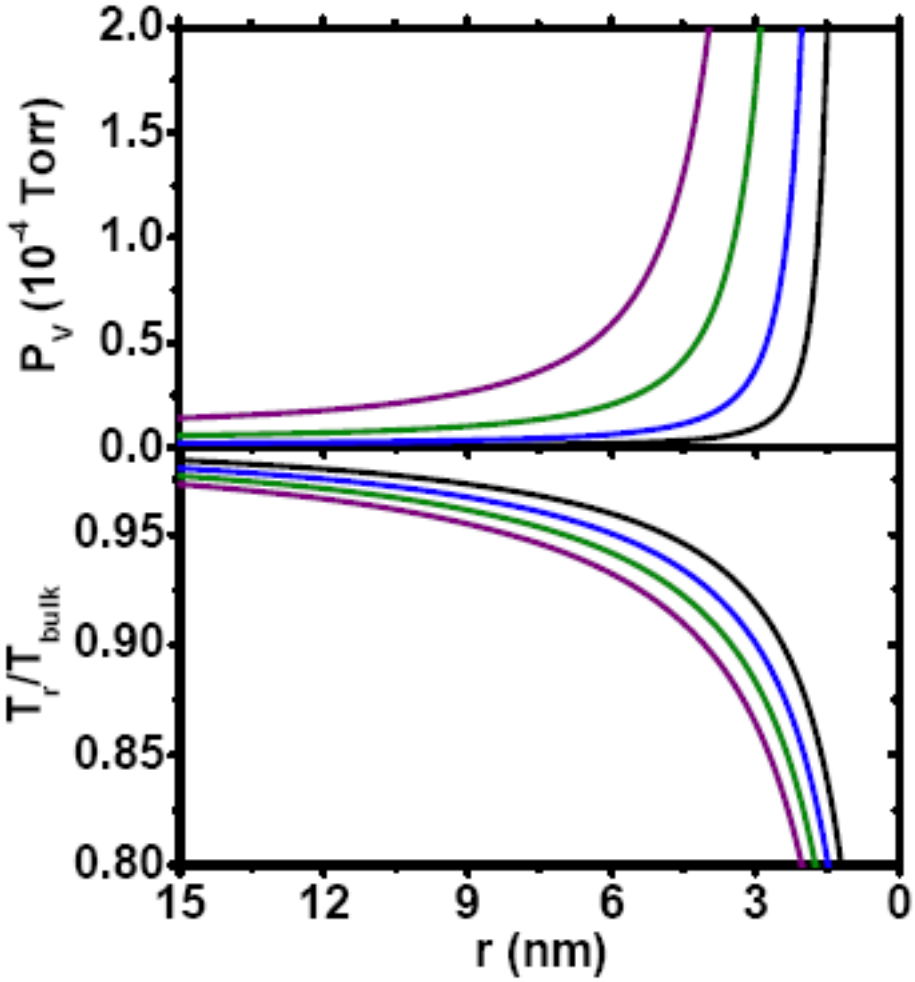

Figure 3 LE13579 04AUG2011

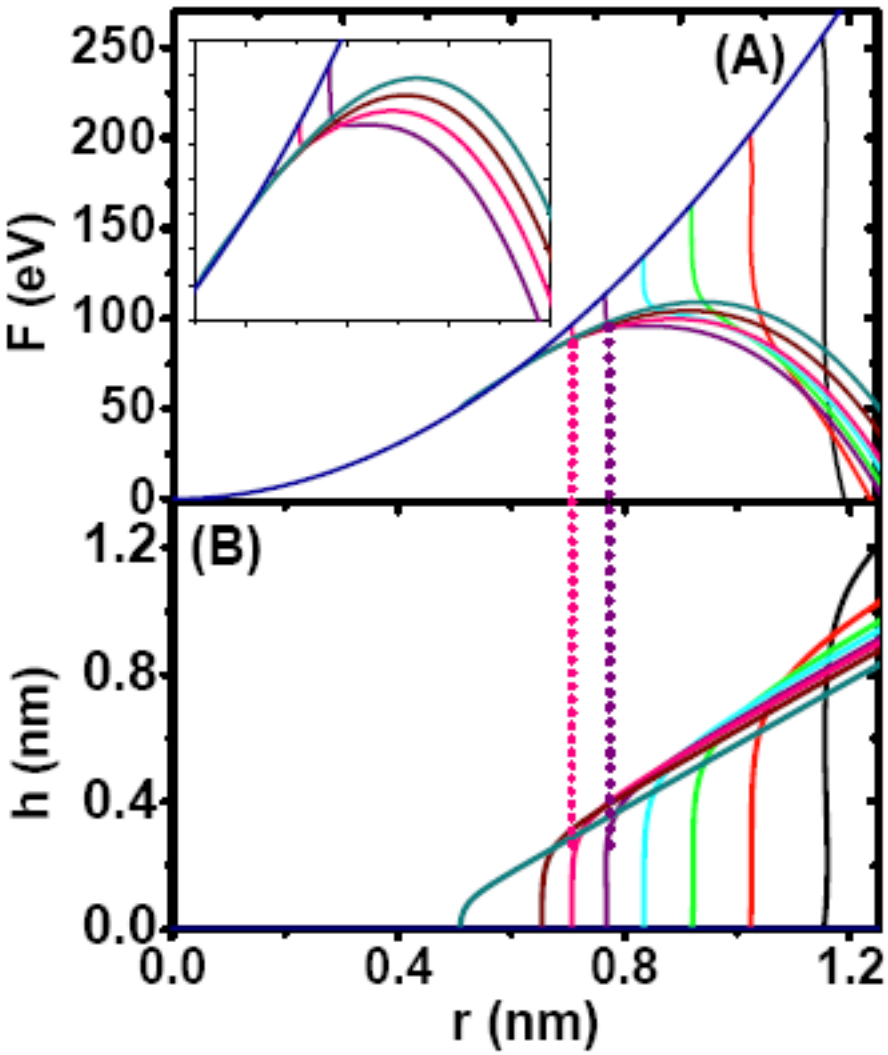

Figure 4 LE13579 04AUG2011